The Brahmaputra tale of tectonics and erosion: Early Miocene river capture in the Eastern Himalaya

Laura Bracciali[1,2,*], Yani Najman[2], Randall R. Parrish[1,3], Syed H. Akhter[4] and Ian Millar[1]

[1]*NERC Isotope Geosciences Laboratory, British Geological Survey, Keyworth, Nottingham, United Kingdom*

[2]*Lancaster Environment Centre, Lancaster University, Lancaster, United Kingdom*

[3]*Department of Geology, University of Leicester, Leicester, United Kingdom*

[4]*Department of Geology, University of Dhaka, Dhaka, Bangladesh*

* Corresponding author

E-mail addresses: laurabrac74@gmail.com (L. Bracciali), y.najman@lancaster.ac.uk (Y. Najman), rrp@bgs.ac.uk (R.R. Parrish), shakhter@univdhaka.edu (S.H. Akhter), ilm@bgs.ac.uk (I.Millar).

ABSTRACT

The Himalayan orogen provides a type example on which a number of models of the causes and consequences of crustal deformation are based and it has been suggested that it is the site of a variety of feedbacks between tectonics and erosion. Within the broader orogen, fluvial drainages partly reflect surface uplift, different climatic zones and a response to crustal deformation. In the eastern Himalaya, the unusual drainage configuration of the Yarlung Tsangpo–Brahmaputra River has been interpreted either as antecedent drainage distorted by the India-Asia collision (and as such applied as a passive strain marker of lateral extrusion), latest Neogene tectonically-induced river capture, or glacial damming-induced river diversion events.

Here we apply a multi-technique approach to the Neogene paleo-Brahmaputra deposits of the Surma Basin (Bengal Basin, Bangladesh) to test the long-debated occurrence and timing of river capture of the Yarlung Tsangpo by the Brahmaputra River. We provide U-Pb detrital zircon and rutile, isotopic (Sr-Nd and Hf) and petrographic evidence consistent with river capture of the Yarlung Tsangpo by the Brahmaputra River in the Early Miocene. We document influx of Cretaceous-Paleogene zircons in Early Miocene sediments of the paleo-Brahmaputra River that we interpret as first influx of material from the Asian plate (Transhimalayan arc) indicative of Yarlung Tsangpo contribution. Prior to capture, the predominantly Precambrian-Paleozoic zircons indicate that only the Indian plate was drained. Contemporaneous with Transhimalayan influx reflecting the river capture, we record arrival of detrital material affected by Cenozoic metamorphism, as indicated by rutiles and zircons with Cenozoic U-Pb ages and an increase in metamorphic grade of detritus as recorded by petrography. We interpret this as due to a progressively increasing contribution from the erosion of the metamorphosed core of the orogen. Whole rock Sr-Nd isotopic data from the same samples provide further support to this interpretation. River capture may have been caused by a change in relative base level due to uplift of the Tibetan plateau. Assuming such river capture occurred via the Siang River in the Early Miocene, we refute the “tectonic aneurysm” model of tectonic-erosion coupling between river capture and rapid exhumation of the eastern syntaxis, since a time interval of at least 10 Ma between these two events is now demonstrated. This work is also the first to highlight U-Pb dating on detrital rutile as a

powerful approach in provenance studies in the Himalaya in combination with zircon U-Pb chronology.

Keywords: Brahmaputra; Yarlung Tsangpo; Eastern Himalaya; river capture; U-Pb chronology; rutile.

1. Introduction

Studies of crustal-scale orogenic systems provide important insights into processes of intra-continental deformation and the dynamic links between continental tectonics, surface processes, climate feedbacks and the biosphere on a global scale. The extent, rate and timing of erosion influence the metamorphic and structural evolution of mountain belts (England and Richardson, 1977; Beaumont et al., 1992; Willett et al., 1993) as well as influencing their exhumation pattern and rate (e.g. Beaumont et al 2001; Zeitler et al., 2001a; Robl et al., 2008). In this context, the investigation of fluvial drainage evolution provides a key to understanding tectonic-erosion interactions. Importantly, the reorganization of drainage systems can also heavily affect the nature, magnitude and spatial distribution of sediment supply to sedimentary basins by significantly changing the size of the hinterland catchment area.

In the eastern Himalaya, assessment of paleodrainage networks has been used to document crustal strain (Hallet and Molnar, 2001) and surface uplift (Clark et al., 2004; Stüwe et al., 2008). In this region the modern Yarlung Tsangpo River, one of the main rivers of Asia, flows east along the suture zone which separates the Indian plate in the south from the Asian plate to the north, then crosses the Namche Barwa massif of the eastern Himalayan syntaxis where it bends sharply south, traverse to the Himalaya as the Siang River and finally flows to the Bengal plains as the Brahmaputra River (Fig. 1).

Considerable debate has existed as to whether the Yarlung Tsangpo–Brahmaputra paleodrainage: i) having maintained its current routing without river capture was antecedent to Himalayan orogenesis (Harrison et al., 1992 and references therein); ii) was antecedent to the development of the Namche Barwa syntaxis (that occurred < 4 Ma according to Seward and Burg, 2008; see also Lang and Huntington, 2014); or iii) whether the Yarlung Tsangpo originally flowed southeast and eventually connected to the Brahmaputra via one or more capture events (e.g. Seeber and Gornitz, 1983; Brookfield, 1998; Clark et al., 2004; Cina et al., 2009; Chirouze et al., 2012a). Some authors have even suggested that the Yarlung Tsangpo may have reversed its flow (Burrard and Hayden, 1907; Cina et al., 2009).

In this paper we use the term *river capture* (also known as *river piracy*) to indicate the type of drainage rearrangement (i.e. transfer of a river's flow to another river) that occurs with the interception of a river by an adjacent river which is experiencing aggressive headward erosion (Bishop, 1995). The point at which river capture is considered to have occurred is taken to be indicated by a sharp change in channel direction, known as the elbow of capture, and implies capture of both the catchment area and the drainage lines (the drainage network) above the elbow. Considerably lower elevation of the capturing stream is essential to provide the steep headwater gradients necessary for stream piracy. The other two types of drainage reorganisation (Bishop, 1995) are *river diversion* (redirection of drainage into an adjacent catchment by a range of mechanisms of divide breaching, including channel migration, tectonic processes such as tilting or doming, or catastrophic avulsion by high magnitude water flows) and *river beheading* (the appropriation of a river's catchment area to an adjacent river without preservation of the appropriated catchment's area drainage lines that results, for example, in truncated valleys hanging in the escarpment as a result of escarpment retreat).

The river capture of the Yarlung Tsangpo by the Brahmaputra has been cited as the cause of the recent rapid exhumation and young metamorphism of the Namche Barwa syntaxis (the proposed site of capture, Fig. 1), and is thought to be an example of tectonic-erosion coupling (Zeitler et al., 2001b). However, independent tests of the occurrence and timing of river capture are sparse and a general consensus has not been reached. Seeber and Gornitz (1983), although arguing for a general antecedence of the Himalayan rivers with respect to the Himalayan topography, did not rule out a possible capture of an ancestral Yarlung Tsangpo–Lohit River by the Brahmaputra. Brookfield (1998) suggested that an ancestral Tsangpo-Irrawaddy was truncated by headward erosion from the Brahmaputra not earlier than the Late Miocene. According to Zeitler et al. (2001b) the rapid fluvial incision likely following capture of the Yarlung Tsangpo by the Brahmaputra caused the very rapid recent exhumation of the Indian plate metamorphic rocks of the Namche Barwa syntaxis during the Plio-Pleistocene. Clark et al. (2004) suggested that the Yarlung Tsangpo was sequentially captured by the paleo-Red, Irrawaddy and Lohit Rivers, before its final capture by the Brahmaputra occurred prior to 4 Ma, based on the proposed age of the localised uplift of the Namche Barwa syntaxis, whilst Seward and Burg (2008) argued for the existence of an antecedent Yarlung Tsangpo–Brahmaputra drainage probably since ~20 Ma.

Cina et al. (2009) and Chirouze et al. (2012a) observe Transhimalayan arc provenance in the Siwalik foreland basin south-west of the syntaxis by 7 Ma while Lang and Huntington (2014) possibly by 13 Ma (based on the correlation to the dated Siwaliks section of Chirouze et al., 2012b). Each of the three studies speculates on alternative scenarios for the evolution of the Yarlung Tsangpo, requiring either a transverse river (such as the Kameng or Subansiri) or a paleo-Yarlung Tsangpo–Brahmaputra (antecedent according to Lang and Huntington, 2014 or not antecedent according to Cina et al., 2009 to the growth of the Namche Barwa syntaxis) to deliver Transhimalayan Arc-derived detritus to the Siwalik foreland basin. These models are further discussed at the end of section 5.

We have applied a multi-disciplinary approach (including whole rock petrographic and isotopic data and detrital single grain U-Pb dating) to the paleo-Brahmaputra sedimentary record preserved in the northern Bengal Basin (Surma Basin, Fig.1) in order to constrain the paleodrainage evolution of the Brahmaputra. In particular we address whether capture of the Yarlung Tsangpo occurred and if so when this happened. Finally, we interpret our results in the wider context of regional Himalayan tectonic events.

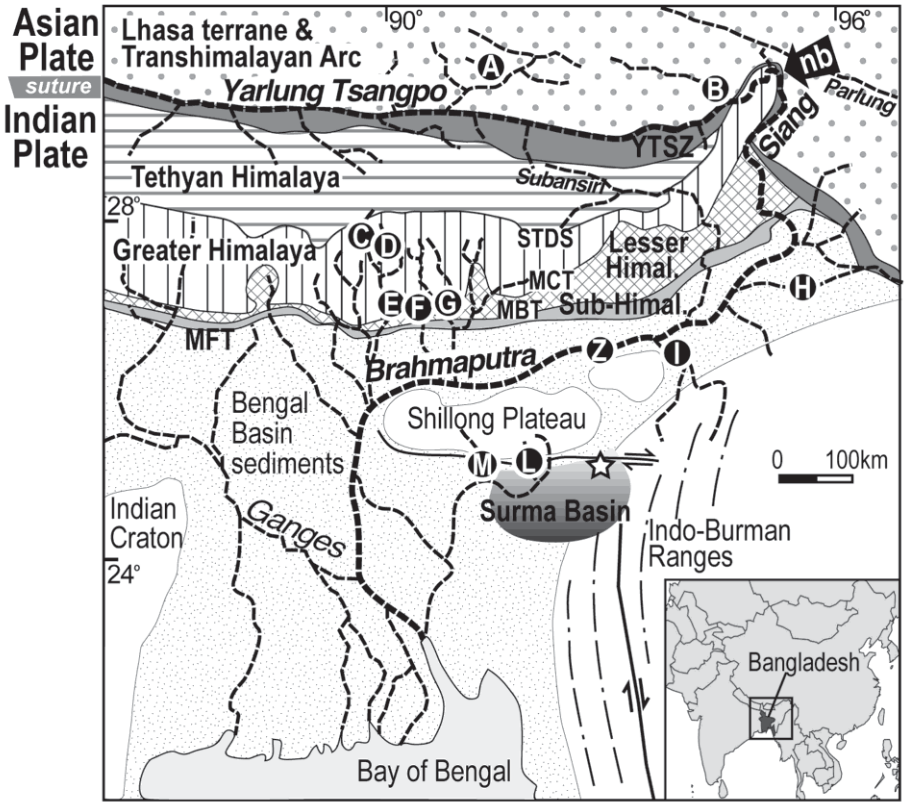

Fig. 1. Major fluvial drainages of the Eastern Himalayan region superimposed on a schematic geological map (Najman, 2006). Location of the represented region in Eastern Asia is shown in inset. Yarlung Tsangpo Suture Zone (YTSZ) separates Asian (Lhasa terrane and the Transhimalayan Arc) from Indian plate (Tethyan, Greater, Lesser and Sub-Himalaya). nb: Namche Barwa massif and site of the proposed capture; STDS : South Tibetan Detachment System; MCT, MBT, MFT: Main Central, Boundary and Frontal Thrusts. Sand sampling locations along modern rivers: A: Lhasa River tributary; B: Niyang; C: Mo Chu; D: Pho Chu; E: Puna Tsang Chu; F: Mangdi Chu; G: Mau Khola; H: Burhi Dihing; I: Dhansiri; Z: Brahmaputra; L: Dauki; M: Jadhu Kata. Star in Surma Basin indicates location of sampling area (see Supplemental Fig. S1 for further details).

2. Geology of the modern-day Yarlung Tsangpo–Brahmaputra catchment

The Ganges and Yarlung Tsangpo–Brahmaputra rivers drain the Himalaya and converge in Bangladesh to form one of the world’s largest sub-aerial fluvio-deltaic systems (the present-day

Bengal Basin, Fig. 1) and the world's largest submarine fan system (the Bengal Fan). The Yarlung Tsangpo originates in Tibet and flows eastwards along the Indus-Tsangpo Suture Zone that separates the Indian plate from the Asian Plate (Fig. 1; see Hodges, 2000; Yin, 2006 and Yin et al., 2010a, for a review of Himalayan geology). North of the suture lies the Lhasa terrane, the southernmost of the four continental blocks comprising the Tibetan Plateau, and the Jurassic–Paleogene Transhimalayan Arc resulting from the northward subduction of the Neo-Tethys slab along the southern margin of Asia (Harris et al., 1990; Copeland et al., 1995). The basement of the Lhasa terrane is comprised of Precambrian gneisses and Paleozoic to Mesozoic sedimentary covers (Zhu et al., 2011).

South of the suture, the South Tibetan Detachment System separates the Tethyan Himalaya (TH, mainly a Paleozoic–Eocene sedimentary succession which was deposited on the northern passive margin of India) from the Indian plate rocks of the Greater Himalaya (GH), metamorphosed across amphibolite to lower granulite-facies conditions during the Cenozoic orogeny (Kohn, 2014). Burial and heating of GH culminated in crustal melting and emplacement of Neogene leucogranites (Guo and Wilson, 2012). The Main Central Thrust separates GH from the Lesser Himalaya (LH, mainly Proterozoic metasedimentary sequence, typically greenschist facies or unmetamorphosed sedimentary cover deposited on Indian crust). The Sub-Himalaya consists of Ceonozoic foreland basin sediments lying between LH and the active thrust front of the orogen (Hodges, 2000).

3. The paleo-Brahmaputra sedimentary record (Surma Basin)

Most of the Bengal Basin fill consists of sediments fluvially transported by the Ganges and Brahmaputra and their ancestral river systems (e.g. the "proto-Ganges Brahmaputra river systems" of Roybarman, 1983; Johnson and Nur Alam, 1991; Reimann, 1993; Uddin and Lundberg, 1998; 1999; Najman et al., 2008; Najman et al., 2012). The Surma Basin (Fig. 1), a sub-basin of the Bengal Basin in north-eastern Bangladesh, is bordered to the north by the Shillong Plateau, the only raised topography in the foreland of the Himalaya, that consists of Indian plate Precambrian basement partially overlain by Cenozoic sediments (Yin et al., 2010b). To the east the Surma Basin is bordered by the Cenozoic Indo-Burman Ranges fold and thrust belt which is propagating west and is responsible for the north-south trending folding in the Bengal Basin. To the west, the adjacent highland is the Precambrian Indian plate, and to the south the region drains to the Bay of Bengal.

The 16 km-thick succession of Eocene-Pleistocene limestone and clastic rocks preserved in the Bengal Basin was deposited on the Indian continental margin that includes the Surma Basin (Fig. 1). Above the Eocene Sylhet Formation limestone and Kopili Formation black shale, the Oligocene-Early Miocene deltaic sandstone of the Barail Formation record the first major clastic influx from the Himalaya (Najman et al., 2008). Above the Barail Formation (Fig. 2) lies the Neogene Surma Group (Bhuban and Bokabil Formations) and the Tipam and Dupi Tila Formations which show facies evolution from deltaic to fluvial environments (Johnson and Nur Alam, 1991; Fig. 2). Earlier dating of the Bengal Basin Formations by lithostratigraphic correlation with rocks far to the north in Assam (Evans, 1932) proved problematic within a deltaic system with high rates of subsidence and rapid facies changes. The samples from this study (Supplemental Table S1) were checked for occurrence of foraminifera, but proved to be either barren or containing sporadic reworked or badly preserved long-ranging benthic species. In order to overcome the limitations of the lithostratigraphic approach, we adopt the seismo-stratigraphic correlation approach of Najman et al. (2012). According to this approach, the Neogene succession has been divided into seismically distinct, unconformity-bounded and regionally correlatable Megasequences (MS in Fig. 2). MS1 is equivalent to the Bhuban and Bokabil Formations, MS2 to the Tipam and Dupi Tila Formations and MS3 is not represented in the Surma Basin. In this basin the boundary between the marine-deltaic seismic megasequence MS1 and the fluvial MS2 lies within nannoplankton zones NN15-NN16, in agreement with a magnetostratigraphic date of 3.5 Ma (Worm et al., 1998). The top of MS2 lies within zones NN19-NN20 and is constrained at 1.4 Ma in the study area by magnetostratigraphy (Worm et al., 1998). The Early Pliocene age for the upper Bhuban Formation is indicated by stratigraphic (Lietz and Kabir, 1982) and magnetostratigraphic data (Worm et al., 1998). The lower boundary of MS1 is constrained at <18 Ma by the occurrence of detrital white mica in uppermost Barail and lowermost Bhuban samples dated by Ar-Ar at 21 ±3 (Najman et al., 2008) and 14±4 Ma (Bracciali, unpublished data), respectively. This is in agreement with prominent modes of Ar-Ar white mica dates of 16–18 Ma in Bhuban samples from well penetrations (Uddin et al., 2010), in which the youngest mica grains in three Bhuban samples of increasing stratigraphic depth are dated at 12.3 ± 0.6 Ma (upper Bhuban, well Beani-Bazar-1X; cf. well stratigraphy in Reimann, 1993), 16.8±0.6 Ma and 19.3±0.8 (lower Bhuban, well Fenchuganj-2; cf. well stratigraphy in Deb et al., 2014). The base of the Barail Formation is constrained at 38 Ma by biostratigraphy (Najman et al., 2008).

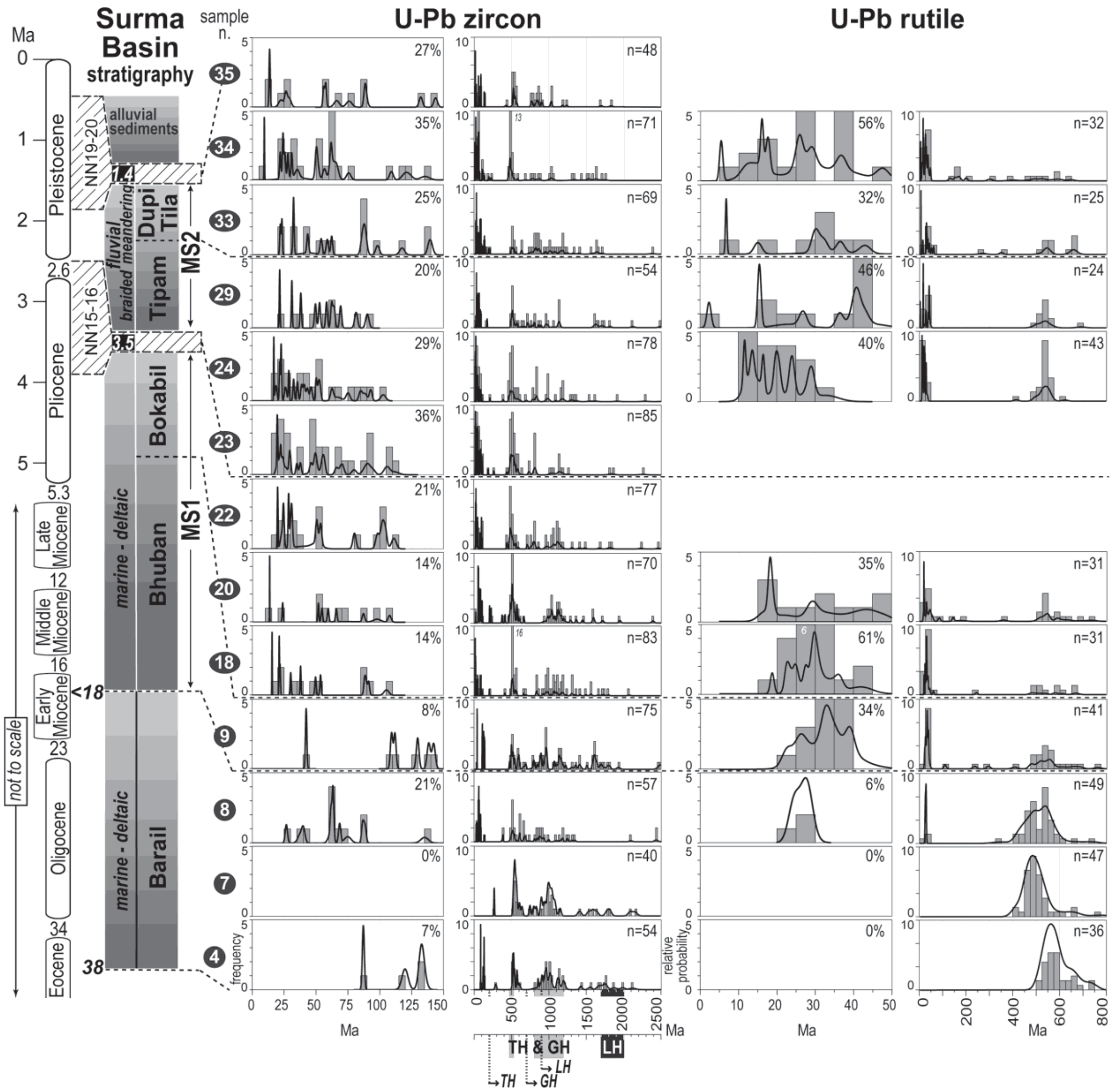

Fig. 2. Surma Basin schematic stratigraphy and detrital U-Pb data from this study. The stratigraphic boundaries are constrained with variable degree of confidence as detailed in main text by biostratigraphy (Lietz and Kabir, 1982; Najman et al., 2012; NN: nannoplankton zones), magnetostratigraphy (Worm et al., 1998) and detrital mineral dates (Najman et al., 2008; Uddin et al., 2010). MS: Megasequence. See Supplementary Material for sample description and U-Pb data. Relative probability plots and frequency diagrams of zircon and rutile single grain U-Pb data are plotted in the range 0–150 and 0–50 Ma, respectively, and in the 0–2.5 and 0–0.8 Ga range. Percentages: number of grains younger than 150 and 50 Ma as compared to n, the total number of individual ablations after rejection of discordant zircon

datapoints (Supplemental Table S2) and common Pb correction of discordant rutile datapoints (as described in Bracciali et al., 2013; Supplemental Table S4). Concordia diagrams are in Supplemental Fig. S4. Light and dark grey bands represent the main age peaks of detrital zircons in TH, GH, and LH based on literature data; dashed vertical lines indicate the youngest populations generally found in the same formations in the eastern Himalaya (see text for references and cf. Fig. 3).

Whilst most workers are in agreement that the majority of the Neogene sediment in the Bengal Basin is Himalayan-derived (e.g. Johnson and Nur Alam, 1991; Uddin and Lundberg, 1998; Uddin et al., 2010), there is considerable debate as to the degree of input from the Indo-Burman Ranges and Shillong Plateau, the timing of river capture when material from north of the suture zone first entered the basin, and the time when the Brahmaputra diverted west of the Shillong Plateau (Johnson and Nur Alam, 1991; Brookfield, 1998; Zeitler et al., 2001a; Clark et al., 2004; Cina et al., 2009; Uddin et al., 2010; Chirouze et al., 2012a).

4. Methods

4.1 Laser Ablation U-Pb dating of zircon and rutile

Laser ablation (LA) U-Pb data were collected at the NERC Isotope Geosciences Laboratory (NIGL) using either a 193 nm or a 213 nm wavelength laser ablation system coupled to a Nu Plasma HR multiple-collector inductively coupled plasma mass spectrometer (MC-ICP-MS). The mass spectrometer used has a specially designed collector block to allow simultaneous detection of all masses in the range 202–207, 235 and 238. Methods followed those described in Thomas et al. (2010). Instrument parameters used during analysis are detailed in Supplemental Table S5. Analysis was performed using the Time Resolved Analysis (TRA) mode of the Nu Plasma software with signals integrated excluding the first 3–5 s of data and the data normalised and uncertainty propagated offline using an in-house Excel spreadsheet. After an initial 30 s instrument baseline measurement and 30 s gas blank, individual analysis ablation times were 40 s for a run of 10–15 ablations. The simultaneous measurement of the ^{202}Hg signal allows correction for the isobaric interference of ^{204}Hg on ^{204}Pb during the ablation. A desolvating nebuliser (DSN-100, Nu Instruments) was used to simultaneously aspirate a solution containing Tl (with isotopes 203 and 205) and ^{235}U in order to correct for mass spectrometer-related mass bias (Pb/Pb ratios using $^{205}Tl/^{203}Tl$, Pb/U ratios using $^{205}Tl/^{235}U$) at the time of analysis. Elemental fractionation from other sources (laser- and plasma-induced) was corrected by comparison of laser ablation data for a primary reference material to ID-TIMS data.

Uncertainties for the $^{207}Pb/^{206}Pb$ ratios were propagated using quadratic addition to combine the measurement uncertainty with a reproducibility component modelled to reflect increasing uncertainty with decreasing signal size. A minimum uncertainty of 0.5% (2σ) was assigned to the $^{207}Pb/^{206}Pb$ ratio by default for ablations with high ^{207}Pb ion beams, to reflect the confidence in the ability of the multi-ion counting (MIC) set-up to accurately reproduce any one value. $^{206}Pb/^{238}U$ uncertainties were propagated in a similar way utilising the measurement uncertainty and the reproducibility of the ablation reference material used.

During each analytical session both zircon and rutile reference materials were measured between each group of unknowns to determine the degree of elemental fractionation, to monitor the effect of matrix on the degree of elemental fractionation, and to assess instrumental accuracy (Supplemental Tables S2, S4 and S5).

Cathodoluminescence images of all zircons were acquired prior to LA work and both cores and rims were analysed. Where thin rims < 10–5 μm were identified on CL images, the grain was removed from mount and the outer surface ablated. Discordant zircon datapoints (Supplemental Figures S3 and S4 and Tables S2 and S4) were not included in the probability plots of Figures 2 and 3. Discordant rutile datapoints were common Pb corrected as described in Bracciali et al. (2013). When two zircon or rutile dates from the same grain overlapped within uncertainty, only the one determined with the lower uncertainty was included in the final probability plot.

4.2 Zircon Hf isotope analysis

Isotope analyses were carried out at NIGL using a Thermo Scientific Neptune Plus MC-ICP-MS coupled to a New Wave Research UP193FX Excimer laser ablation system and low-volume ablation cell. Helium was used as the carrier gas through the ablation cell with Ar make-up gas being connected via a T-piece and sourced from a Cetac Aridus II desolvating nebulizer. After initial set-up and tuning a 2% HNO_3 solution was aspirated during the ablation analyses. Lutetium (^{175}Lu), Ytterbium (^{172}Yb, ^{173}Yb), and Hafnium (^{176}Hf, ^{178}Hf, ^{179}Hf and ^{180}Hf) isotopes were measured simultaneously during static 30 s ablation analyses (50 µm; fluence = 8–10 J/cm^2).

Hf reference solution JMC475 was analyzed during the analytical session and sample ^{176}Hf/^{177}Hf ratios are reported relative to a value of 0.282160 for this standard (Supplemental Table S3). Correction for ^{176}Yb on the ^{176}Hf peak was made using reverse-mass-bias correction of the ^{176}Yb/^{173}Yb ratio empirically derived using Hf mass bias corrected Yb-doped JMC475 solutions. ^{176}Lu interference on the ^{176}Hf peak was corrected by using the measured ^{175}Lu and assuming ^{176}Lu/^{175}Lu = 0.02653. Two zircon reference materials (91500 and Mud Tank) were analysed throughout the analytical session. 16 analyses of Mud Tank gave a mean ^{176}Hf/^{177}Hf value of 0.282515 ± 0.000013 (1σ). 48 analyses of the 91500 reference material showed considerably more scatter, with a mean value of 0.282309 ± 0.000021 (1σ). 91500 zircon reference material was used to normalise the ^{176}Lu/^{177}Hf ratio assuming a value of 0.000311.

Analytical uncertainties for unknowns were propagated by quadratic addition to include the standard error of the mean of the analysis and the reproducibility of the Mud Tank reference material.

4.3 Modal analysis of sandstones

In each arenite sample 400 points were counted at the British Geological Survey, Nottingham, by the Gazzi-Dickinson method (Ingersoll et al., 1984) to minimise the dependence of arenite composition on grain size. Calculated grain parameters are presented in Supplemental Table S6. Metamorphic lithic grains were classified according to protolith composition and metamorphic rank (Garzanti and Vezzoli, 2003). Average rank for each sample was expressed by the "Metamorphic Index" MI, which varies from 0 in detritus from sedimentary and volcanic cover rocks to 500 in detritus from high-grade basement rocks (Garzanti and Vezzoli, 2003). Very low to low-rank metamorphic lithics, for which protolith can still be inferred, were subdivided into metasedimentary (Lms) and metavolcanic (Lmv) categories. Medium to high-rank metamorphic lithics were subdivided into felsic (metapelite, metapsammite, metafelsite; Lmf) and mafic (metabasite; Lmb) categories.

4.4 Whole rock Sr and Nd isotope analysis

For Sr and Nd analysis, powders obtained from samples were leached at NIGL in 10% acetic acid in order to remove carbonate. Subsequently, the samples were spiked with ^{84}Sr and ^{150}Nd isotope tracers and dissolved using HF and HNO_3. After an initial separation using Dowex AG50X8 cation exchange resin, Sr was separated using EICHROM Sr-Spec resin, and Nd was separated using LN-Spec resin. Sr was loaded on single Rhenium filaments using a TaO activator and analysed in multidynamic mode on a Thermo Triton mass spectrometer. Nine analyses of SRM987 gave a mean $^{87}Sr/^{86}Sr$ value of 0.710250 ± 0.000006 (1σ). Nd was loaded on rhenium double filaments and analysed in multidynamic mode on a Thermo Triton mass spectrometer. Five analyses of the La Jolla standard gave a mean $^{143}Nd/^{144}Nd$ value of 0.511847 ± 0.000007 (1σ).

5. Early Miocene river capture of the Yarlung Tsangpo by the Brahmaputra River

As detailed in section 2, the Asian plate, along which the Yarlung Tsangpo flows, contains a very different geology to the Indian plate, which would have been the predominant contributing source region of the paleo-Brahmaputra prior to the river capture of the Yarlung Tsangpo. Distinctive of the southern margin of the Asian plate are the pre-collisional Jurassic-Paleogene subduction-related granitoids of the Transhimalayan batholiths intruding the Lhasa Terrane (see review in Zhu et al., 2011). The Linzizong volcanics (~65–45 Ma), the effusive products of the Transhimalayan magmatic activity in the southern Lhasa terrane, consist of an east-west linear belt of calc-alkaline andesitic flows, tuffs and breccias, dacitic to rhyolitic ignimbrites and hypabyssal rocks (Mo et al., 2008). The southern Lhasa terrane also includes younger Cenozoic rocks: potassium-rich mafic rocks (23–8 Ma, Guo et al., 2013) and adakites (30–9 Ma, Chung et al., 2009), that are coeval with Himalayan leucogranites and migmatites (24–15 Ma, Searle et al., 2010; 25–9 Ma, Guo and Wilson, 2012). These rocks are of limited extent compared to the Transhimalayan Arc rocks.

The Indian plate, comprising the Himalayan thrust belt south of the suture zone, mainly consists of metasedimentary rocks of Proterozoic and Paleozoic–Eocene (Tethyan) age, with GH rocks having been metamorphosed to amphibolite-granulite facies in the Oligocene-Miocene (Kohn, 2014) since India-Asia collision ~ 50 Ma (Najman et al., 2010). (Meta-) sedimentary rocks from TH, GH and LH in the eastern Himalayan region yield U-Pb zircon dates older than ca. 200, 700 and 900 Ma, respectively (Aikman et al., 2008; Webb et al., 2013). U-Pb age spectra of detrital TH and GH zircons across the Himalayan orogen exhibit main peaks at ~0.5 and 0.8–1.2 Ga, while in LH spectra the dominant age range is 1.7 to 2.0 Ga (Parrish and Hodges, 1996; DeCelles et al., 2000; McQuarrie et al., 2008; Gehrels et al., 2011; Martin et al., 2011), although zircon grains as young as 0.5 Ma occur in the outer LH (Myrow et al., 2003; McKenzie et al., 2011; Gehrels et al., 2011). U-Pb zircon dates younger than 50 Ma in Paleogene granitoids (e.g. 44 Ma, Aikman et al., 2008; 42–43 Ma, Zeng et al., 2011; 47–30 Ma, Hou et al., 2012) and migmatites (31–17 Ma, Rubatto et al., 2012) intruding the eastern TH and GH testify to a prolonged Eocene-Oligocene phase of crustal melting within the Himalayan orogen. In the Himalaya south of the suture zone, Cretaceous–Paleogene plutonic rocks (in the range ~50–75 Ma) are absent, therefore first evidence of the Asian Transhimalayan Arc detrital material in the Surma Basin constrains the occurrence and timing of river capture.

First we provide U-Pb detrital evidence consistent with river capture of the Yarlung Tsangpo by the Brahmaputra River, documented by arrival in the Surma Basin of Cretaceous–Paleogene zircons (Fig. 2) with predominantly oscillatory zoning typical of volcanic-plutonic rocks derived from the erosion of the Transhimalayan Arc. In addition to zircon U-Pb single grain dating, we report the first published single grain U-Pb dates of detrital rutile from Himalayan-derived deposits of the Bengal Basin and from modern rivers draining the Transhimalayan Arc and Himalaya of the Indian plate. Detrital zircons from modern rivers are used to characterise potential rock sources (Fig. 3).

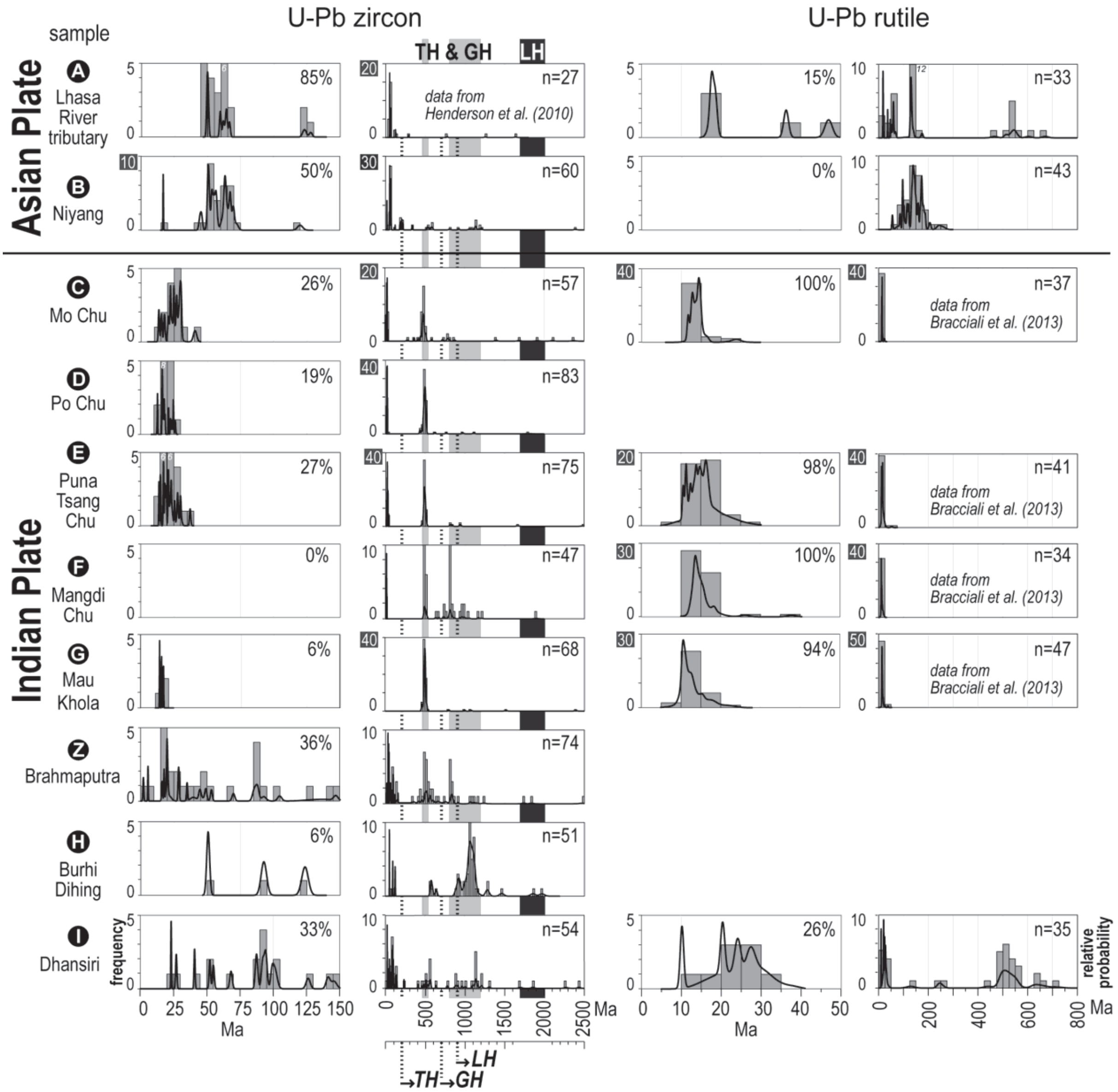

Fig. 3. Detrital U-Pb data of modern river sands from this study (Supplemental Tables S2 and S4) plotted as relative probability and frequency plots. One zircon sample and four rutile samples are from Henderson et al. (2010) and Bracciali et al (2013), respectively. Sample locations (A–I and Z) as shown in Fig. 1; horizontal axes, percentages and n as in Fig. 2. Concordia diagrams are in Supplemental Fig. S3. Light and dark grey bands, plotted for comparison, represent the main age peaks of detrital zircons in TH, GH, and LH based on literature data; dashed vertical lines indicate the youngest populations generally found in the same formations in the Eastern Himalaya (see text for references).

U-Pb dates from single detrital zircons represent high-T igneous and metamorphic events in the source regions, while rutile, a medium-T chronometer, tracks mainly the time of cooling through ~500°C (Bracciali et al., 2013). The two chronometers applied to the same sample provide key complementary information about the thermal events in the source region. Importantly, we use CL imaging to identify and date all zircon growth zones of single grains with a novel approach to dating also very thin (<5 μm) rims. These zircon rims record the latest growth events that otherwise would be missed due to the difficulty in analysing such narrow zones of zircon.

Fig. 3 characterises the isotopic zircon and rutile ages from the potential sources to the Bengal Basin as documented in modern fluvial sediments eroded from the eastern Himalaya of the Indian plate. Samples C-G mainly draining GH in Bhutan are characterised by up to 20% of zircon grains (core and rims) and metamorphic rims 20–40 Ma old and by 10–20 Ma rutiles, documenting Himalayan metamorphism and anatexis (Hodges, 2000). The same samples include zircons older than ~500 Ma with a distinct peak around 480–500 Ma, the reported age of granitic gneisses and granites intruding GH that corresponds to the intrusion of late Pan-African granites (Gehrels et al., 2003; DeCelles et al., 2004; Cawood et al., 2007; Gehrels et al., 2011). The 500 Ma peak also characterises TH and GH as shown by detrital U-Pb published data (Fig. 3). The Burhi Dihing (sample H), an eastern tributary of the Brahmaputra that drains the outer part of the Indo-Burman Ranges, is mainly characterised by > 500 Ma zircons, with a prominent peak at ~ 1 Ga (sample H), while the more southern Dhansiri River (sample I) yields a scatter of Mesozoic and Cenozoic as well as > 500 Ma zircons, and two main rutile age populations at 20 –30 Ma and ~ 500 Ma. Modern detritus of rivers that drain the Shillong Plateau (samples M and L in Fig. 1; data in Najman et al., 2008) yields only Cambrian and Precambrian zircons, with main peaks around 500 Ma and 1.0, 1.2 and 1.6 Ga. The same Precambrian peaks are found in sandstones of the Proterozoic Shillong Group that are intruded by a 480–500 Ma granite (Yin et al., 2010b).

By contrast, the Transhimalayan Arc of the Asian plate (samples A and B) is mainly characterised by zircon U-Pb dates between 50–75 Ma reflecting derivation from pre-collisional subduction-related granitoids, while rutile in this age range or younger is minimal or lacking, with grains exclusively (sample B) or mainly (sample A) 100–200 Ma. The detrital age pattern of the Brahmaputra (sample Z) includes all the different components described above.

In the Surma Basin all zircon samples are characterised by a Cambrian-Ordovician peak (~ 500 Ma) and by a spread of older ages (Fig. 2). In samples 4 and 7, the lowermost and middle Barail samples, a distinct cluster of ~ 1 Ga zircon is present and rutiles are > 400 Ma (Fig.2). The uppermost Barail sample (8; Fig. 2) is the oldest sample to show both Cenozoic-aged detrital zircon rims and rutiles derived from the exhumed metamorphosed core of the Himalaya and 50–75 Ma old zircons characteristic of Transhimalayan igneous input; the latter is further supported by Paleogene-Cretaceous zircon grains with a positive ε_{Hf} isotopic composition which is characteristic from the uppermost Barail sample onwards and consistent with Transhimalayan Arc provenance (Gangdese Batholith, Fig. 4). Such a positive ε_{Hf} signature (also typical of the modern Yarlung Tsangpo main trunk; Zhang et al., 2012) contrasts with the generally negative ε_{Hf} values of the Northern Plutonic Belt, the Eastern Batholiths and the Dianxi-Burma Batholiths (Fig. 4). Some igneous rocks in Burma are characterised by ~50–80 Ma zircons with slightly positive (<5) ε_{Hf} values (the western Yingjiang batholiths of Xu et al., 2012; Y in the diagram of our Fig. 4), hence derivation of some of the Surma Basin zircons from these sources cannot be ruled out. However, the positive ε_{Hf} values of most of the Cretaceous–Paleogene zircons from our samples lend support to our interpretation of the Transhimalayan Arc as the dominant igneous source to the Surma Basin.

Importantly, the youngest detrital rutile U-Pb, mica Ar-Ar and zircon fission track dates of the uppermost Barail sample overlap within analytical error, being respectively 24.4 ± 2.9 (this work), 21.1 ± 3.2 and 23 ± 2 Ma (the latter is the youngest age component of the sample; Najman et al., 2008). Under the assumption of erosion of these different mineral grains from a common source area, these data indicate rapid cooling of the source through ~500 –200 °C, hence the depositional age of our uppermost Barail sample is expected to be not much younger than the cooling age of its detrital components (Early Miocene). Rapid orogenic exhumation consistent with progressive erosion to deeper levels of the southern flanks of the Himalayan orogen is observed in the whole Barail formation, as evidenced for example by the short lag time between sediment depositional age of the lowest Barail (38 Ma, biostratigraphic age) and the fission track date of the youngest detrital zircon population (37 ± 2 Ma) from a sample a few tens m above (Najman et al., 2008).

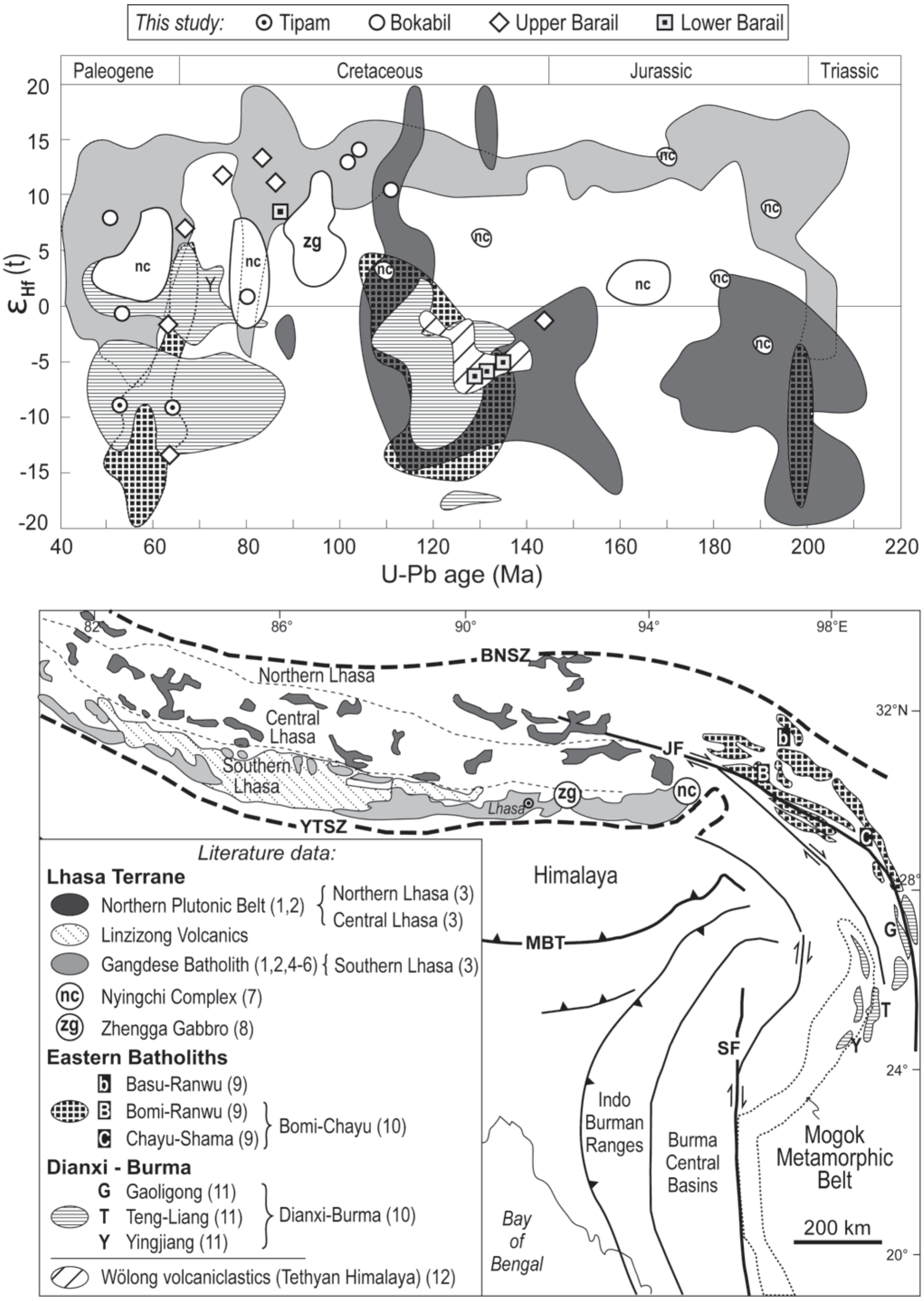

Fig. 4. Plots of initial ε_{Hf} versus U-Pb data of selected zircon samples from the Surma Basin compared to potential bedrock igneous sources from the Himalayan-Tibet-Burma region. (1) Chu et al. (2006); (2) Zhang et al. (2007); (3) Zhu et al. (2011); (4) Chu et al. (2011); (5) Ji et al. (2009); (6) Ji et al. (2012); (7) Guo et al. (2011); (8) Ma et al. (2013); (9) Chiu et al.

(2009); (10) Liang et al. (2008); (11) Xu et al. (2012). The main geological elements of the region and the location of the igneous rocks are schematically represented on the map (redrawn after Searle et al., 2007; Chiu et al., 2009; Chu et al., 2011; Zhu et al., 2011). Detrital Cretaceous-Paleogene zircons from the Surma Basin characterised by positive initial ε_{Hf} values are consistent with derivation from Asian plate ("Lhasa Terrane"), with most grains overlapping with values typical of the Cenozoic Gangdese Batholith. One negative Cretaceous grain in the upper Barail is compatible with derivation from the Northern Plutonic Belt and three lower Barail 130–145 Ma negative grains are compatible with either the Northern Plutonic Belt, the Eastern Batholiths or recycling of Tibetan TH deposits such as the Wölong volcaniclastics (Hu et al., 2010, reference 12). The Gangdese, the Eastern Himalayan or the Dianxi Burma Batholiths might have sourced the Paleogene zircons with a negative ε_{Hf} signature. BNSZ: Bangong-Nujang Suture Zone; YTSZ: Yarlung Tsangpo Suture Zone; MBT: Main Boundary Thrust; JF: Jiali Fault; SF: Sagaing Fault. Northern, Central and Southern Lhasa according to Zhu et al. (2011).

Samples 7 and 4 from the middle and lower Barail (Fig. 2), and the underlying Eocene Kopili Formation (Najman et al., 2008) lack 50–75 Ma grains but contain a few grains ~87 and 115–135 Ma, the latter identical to the Tethyan Wölong volcaniclastic rocks (Hu et al., 2010) that are part of the Indian plate south of the suture (see the Hf isotopic composition of three of these lower Barail grains in Fig. 4). Intraplate basaltic rocks in Eastern India such as the Rajmahal and Sylhet Traps (Baksi, 1995) have been indicated as potential sources to the Wölong volcaniclastics (Hu et al., 2010). The Sylhet Traps in northeastern India could have also been a primary source of detritus for the lower Barail Formation.

The contrast between the lower–middle Barail samples (dominated by Precambrian to Cambrian zircon and rutile grains and total lack of 50–75 Ma zircons) and the overlying samples (with increasingly dominant and upwards-younging Late Cretaceous–Cenozoic zircon and Cenozoic rutile populations, Fig. 2) indicates a major change in provenance which we interpret as resulting from the

the river capture of the Yarlung Tsangpo by the Brahmaputra River. This potentially occurred via the transient capture of one or more transverse Himalayan rivers as discussed later in this section. The capture must have taken place prior to the deposition of our uppermost Barail sample, the first to show the Transhimalayan Arc provenance signature and whose stratigraphic age is likely not much younger than 21-18 Ma as discussed earlier in this section. Our data thus constrain the first arrival of Transhimalayan material into the Surma Basin. This was accompanied by enhanced input from the metamorphosed Himalaya (as evidenced from appearance of Cenozoic rutiles) when the GH high grade metamorphic rocks began to be eroded since ca 23–20 Ma (Hodges, 2000). The continuation in the trend of youngest rutile and zircon U-Pb dates upsection reflects continued exhumation to progressively deeper levels of the Himalayan source region, thus ruling out recycling as a major process contributing sediment to the Surma Basin.

The petrographic composition of the Surma Basin sandstones since the Early Miocene (upper Barail to Dupi Tila; Fig. 5) indicates gradual relative decrease of quartz and increase upsection of feldspar and lithic grains (cf. Fig. 5A and Fig. 5B). The same samples show a shift from a composition dominated by sedimentary to low-rank metamorphic lithic grains in the lower–middle Barail (Fig. 5D) to a composion more enriched in volcanic to low-rank metavolcanic and medium- to high-rank metamorphic lithic grains in upper Barail to Dupi Tila deposits (Fig. 5C).

This general increase upsection in feldspar suggests an increasing contribution from crustal rock sources possibly including an arc terrane. Parallel to the increase of feldspar and lithic grains content is the increase of the Metamorphic Index (MI) of the samples (Fig. 6; Garzanti and Vezzoli, 2003). We interpret the increase in MI to reflect progressive erosion into deeper-seated metamorphic units of the growing Himalayan since the Early Miocene (upper Barail time). The contribution from mid-crustal rocks is however less extensive than in modern Brahmaputra sands, characterised by a higher MI (Fig. 6A). This reflects a composition dominated by the erosion of the high grade metamorphic rocks of the eastern syntaxis (accounting for ~ 40% of the total modern Brahmaputra sediment flux, e.g. Garzanti et al., 2004).

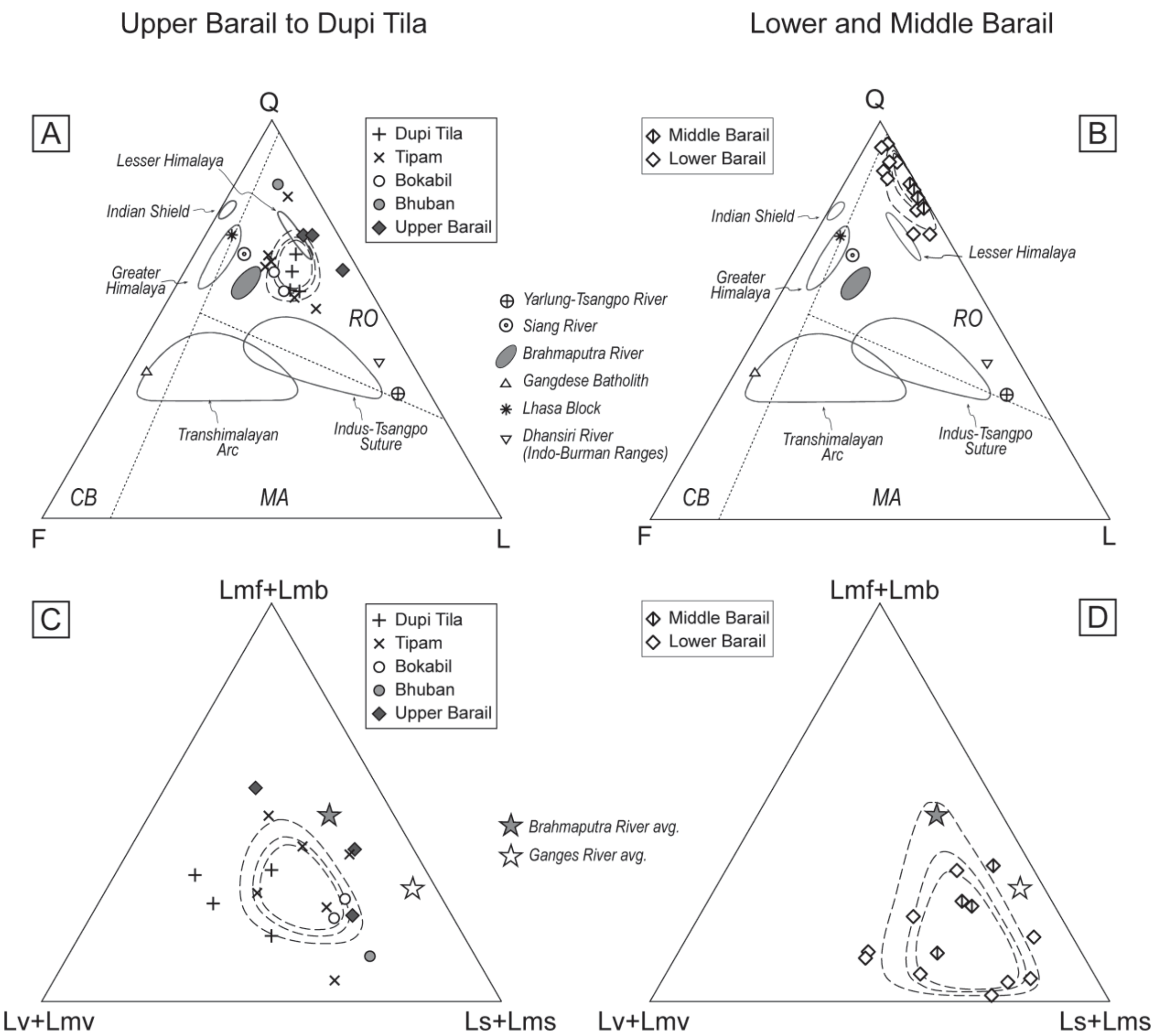

Fig. 5. Modal petrographic data of sandstones from the Surma Basin.

A) and B): Surma Basin sandstones (Supplemental Table S6; Barail data from Najman et al., 2008) plotted on the Q-F-L (total quartzose grains, feldspar grains, lithic grains) ternary diagram (Dickinson, 1982). All samples (carbonate-free feldspatic lithoarenites based on the nomenclature of Dickinson, 1982, variably affected by weathering) plot in the Recycled Orogen (RO) compositional field. CB: continental block; MA: Magmatic Arc. The sand compositions of the Yarlung Tsangpo, Siang, Brahmaputra and other Himalayan Rivers are plotted for comparison (Q-F-(L-Lc) data from Garzanti et al., 2004).

C) and D): same samples plotted on the (Lmf+Lmb,)-(Lv+Lmv)-(Ls+Lms) diagram.

The composition of upper Barail sandstones (lithic arenites) is more similar to the other Neogene samples than to middle and lower Barail samples (sublitharenites to quartz-arenites).

To highlight these differences 90, 95 and 99% confidence regions about the mean (dashed curves, calculated using the software CoDaPac, Comas-Cufí and Thió-Henestrosa, 2011) are shown for the two groups of samples (upper Barail-Dupi Tila and lower-middle Barail).

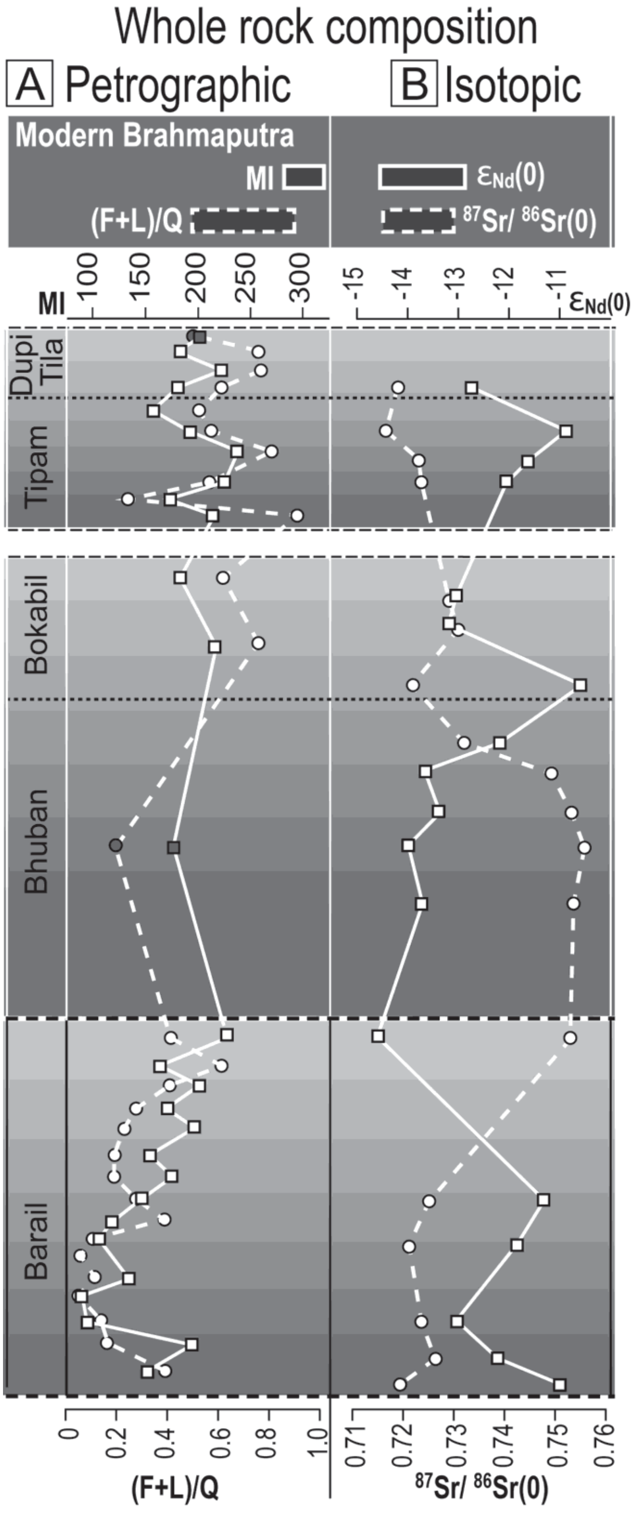

Fig. 6. Overview of petrographic and whole rock isotopic composition of sedimentary samples from the Surma Basin.

A) The ratio (Feldspar+Lithic fragments)/Quartz (dashed line) and the Metamorphic Index of sandstones are plotted (Barail petrographic data from Najman et al., 2008). Thick bars: modern Brahmaputra range of values (Garzanti et al., 2004). The stratigraphic position of two samples (dark filled symbols) is not known with respect to the other samples from the same formation.

B) Whole rock Sr-Nd composition of sandstone and mudstone samples from the Surma Basin. Sr data: dashed line. Thick bars: modern Brahmaputra range of values (Singh and France-Lanord, 2002).

Whole rock Sr–Nd isotopic data mimic the compositional changes shown by the petrographic data (Fig. 6B and Fig. 7). Overall, the Barail to Dupi Tila samples are characterised by Sr and Nd isotopic compositions that can result from the mixing of different proportions of end-member compositions from the Tibet-Himalaya region (Fig. 7).

Five Lower-Mid Barail samples (Fig. 6B) have a rather homogeneous isotopic signature (0.72 to 0.73 and -11 to -13). The $^{87}Sr/^{86}Sr(0)$ and $\varepsilon_{Nd}(0)$ signature of these samples is interpreted as predominantly TH- and GH-derived (Fig. 7) and is consistent with the composition of Himalayan-derived Eocene rocks of the foreland basin in Nepal (e.g. Robinson et al., 2001). The uppermost Barail sample starts a new trend characterised by a progressive shift through time towards modern Brahmaputra values (Fig. 6B). This sample is characterised by more radiogenic $^{87}Sr/^{86}Sr(0)$ ratios coupled to more negative $\varepsilon_{Nd}(0)$ values than the underlying Barail samples(~ 0.75 and -14, Fig. 6B; note that this is the same uppermost Barail sample, number 8, shown in Fig. 2). Consistent with our interpretations from the U-Pb data (Fig. 2) and the petrographic data (Fig. 6A), we interpret this sharp change at the Early Miocene as the result of the accelerated erosional unroofing of older mid-crustal GH metamorphic rocks (Hodges et al., 1996). Further erosion of GH rocks (typical $^{87}Sr/^{86}Sr(0)$ and $\varepsilon_{Nd}(0)$ values: 0.76 and -15; Singh and France-Lanord, 2002) coupled to addition of detritus from the

LH (the Himalayan source with the most extreme isotopic signature with typical $^{87}Sr/^{86}Sr(0)$ and $\varepsilon_{Nd}(0)$ values = 0.85 and -24, Fig. 7) following its exhumation since the Middle-Late Miocene (Najman et al., 2009) should have resulted in an increasingly more radiogenic Sr composition and more negative $\varepsilon_{Nd}(0)$ values of the samples upsection into the Neogene. However, the progressive shift towards present-day Brahmaputra values (Fig. 6B) from upper Barail times onwards indicates that such an input (from GH and LH rocks) must have been significantly buffered by mixing with a source characterised by less radiogenic Sr values and higher $\varepsilon_{Nd}(0)$ values, which we identify as the Transhimalayan Arc (e.g. $^{87}Sr/^{86}Sr(0) < 0.73$ $\varepsilon_{Nd}(0)$ = -10 to +5; Singh and France-Lanord, 2002; Lhasa block volcanics and granitoids in Fig. 7) and suture zone ophiolites (Yarlung Tsangpo Ophiolite in Fig. 7). Such a juvenile component indeed differentiates the modern Brahmaputra (main trunk) isotopic composition ($^{87}Sr/^{86}Sr(0)$ = 0.71–072 and $\varepsilon_{Nd}(0)$ = -14 to -12; Singh and France-Lanord, 2002; Fig. 6B) from the Ganges River ($^{87}Sr/^{86}Sr(0)$ = 0.74–084 and $\varepsilon_{Nd}(0)$ = -25 to -15; Singh et al., 2008) that mainly drains GH.

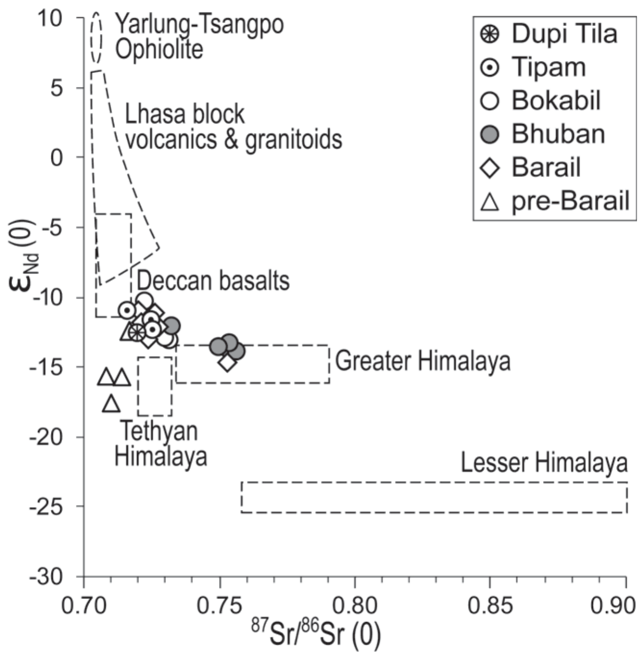

Fig. 7. Whole rock Sr and Nd isotopic data from the Surma Basin.

In this ε_{Nd} vs $^{87}Sr/^{86}Sr$ diagram Surma Basin samples from this study (Supplemental Table S7) and pre- Barail samples from Najman et al. (2008) are plotted along with compositional fields of potential source rocks from the Himalaya-Tibet region (Singh et al., 2008; Wu et al., 2010). The main lithotectonic units of the Himalaya have quite distinct Sr-Nd signatures that are reflected in their erosion products (Singh and France-Lanord, 2002; Parrish and Hodges, 1996; Robinson et al, 2001; Singh et al., 2008; Wu et al., 2010; Galy et al., 2010).

As summarised in the Introduction, considerable debate has existed as to whether the Yarlung Tsangpo–Brahmaputra paleodrainage was antecedent to orogenesis, or whether the Yarlung Tsangpo originally flowed east, sequentially captured by rivers such as the paleo-Red, Irrawaddy and Lohit Rivers, before its final capture by the Brahmaputra. All of the data and interpretations presented in this paper are consistent with Early Miocene capture by the Brahmaputra of a river draining the Asian plate, followed by increased exhumation of GH accompanied by significant input from the Transhimalayan Arc.

Such a dramatic drainage reorganisation occurred either directly via the Siang as in the modern drainage configuration, or involved the sequential capture of one (or more) transverse Himalayan rivers that, differently from the modern ones that drain only the southern slopes of the Himalayan orogen (e.g. the Subansiri, Fig. 1), would have reached the Transhimalayan Arc to the north of the suture. Our detrital data from the paleo-Brahmaputra deposits in the Surma Basin indicate an enduring and stable detrital signature following the establishment of the drainage in the Early Miocene, testifying to significant and increasing erosion of the Asian arc source and high grade Himalayan metamorphic rocks as a major drainage would have provided. The *capture* (Bishop, 1995) of the Yarlung Tsangpo by the Brahmaputra via the Siang, with integration of the highly elevated Yarlung Tsangpo catchment into the Siang–Brahmaputra drainage basin and preservation of its drainage lines, would explain the peculiar drainage configuration in the eastern syntaxis area (Fig. 1), with the sharp bend of the river representing the elbow of capture (although the current river drainage pattern in the Namche Barwa area has also probably been affected to a certain extent by the deformation associated with the development of the syntaxis). However, based on our data, it is difficult to establish if the connection between the Yarlung Tsangpo and the Brahmaputra occurred via the capture of one or more transverse rivers in sequence, as the switch between these rivers, draining similar geological units, would likely have occurred without major perturbation of the detrital signature we observe in the Surma Basin.

Our interpretation of the establishment of the Yarlung Tsangpo–Brahmaputra River in the Early Miocene is strengthened by its consistency with recent provenance studies which utilised detrital zircon U-Pb data from Central Myanmar and Himalayan foreland basins to track the occurrence of detritus from the Yarlung Tsangpo suture zone. Robinson et al. (2014) proposed that an ancestral Yarlung Tsangpo flowed into the Irrawaddy drainage in Central Myanmar until 18 Ma, based on a study which showed the Yarlung Tsangpo suture zone signal was lost from the Irrawaddy basin at that time. This is consistent with the work of Rüber et al (2004) who showed clade divergence of fresh water fish species between the Yarlung Tsangpo and the Irrawaddy regions in the Early Miocene, interpreted to have resulted from a vicariant event, consistent with the palaeodrainage scenario proposed here.

Transhimalayan Arc provenance has been observed in the Arunachal Pradesh part of the Siwalik Group foreland basin in sediments of latest Miocene age (~ 7 Ma), just north of the Shillong Plateau by Cina et al (2009) and Chirouze et al (2012a). This was interpreted as the result of capture of the Yarlung Tsangpo first by the Subansiri River and then by the Siang (Cina et al., 2009) or as the result of surface uplift of the Shillong plateau that pushed the paleo-Yarlung Tsangpo–Brahmaputra, already flowing along the Brahmaputra valley as currently located, north towards the Himalayan front at this time (Chirouze et al., 2012a). More recently, Lang and Huntington (2014) recorded Asian-derived detritus in foreland basin Lower Siwaliks deposits which are generally magnetostratigraphically dated from 10 to 14 Ma, with the transition from Lower to Middle Siwaliks also reported at ~8Ma (Ojha et al., 2009). The age of the stratigraphic section of Lang and Huntington at Likabali, lacking any direct age constraint, is inferred based on correlation to the Kameng River section exposed ~250 Km to the SW, where the Lower Siwaliks sedimentary record extends to ca. 13 Ma due to basal truncation by the Tipi Thrust (Chirouze et al. 2012b). The data of Lang and Huntington (2014) thus suggest the existence of a paleo-Yarlung Tsangpo–Brahmaputra by at least the upper part of Middle Miocene times (note: not Early Miocene as they wrote). As a whole, the work of

Cina et al (2009), Chirouze et al (2012a) and Lang and Huntington (2014) is compatible with a paleo-Yarlung Tsangpo–Brahmaputra flowing along the foreland of the Himalayas at least by 7-13 Ma. This is in agreement with the Sr-Nd-Os isotopic composition of sediment deposited in the last 12 Ma in the Bengal Fan, testifying to a stable erosion pattern in the Himalaya and requiring a stable connection between the Tibetan Plateau and the Bengal Fan such as the Yarlung Tsangpo–Brahmaputra would have provided (Galy et al., 2010). All of these data are consistent with our findings of a Yarlung Tsangpo–Brahmaputra established since the Early Miocene.

6. Conclusions and wider implications

We interpret various changes in provenance in Surma Basin sediments that occurred in the Early Miocene to represent the first arrival of material from the Asian plate, due to river capture of the Yarlung Tsangpo by the Brahmaputra at this time. This river capture may have been caused by an increase in river gradient and stream power due to uplift of the Tibetan plateau, as for example suggested by the numerical modelling of Stüwe et al (2008). It has also been proposed that rapid downcutting of the river may have resulted in the anomalously young metamorphism and recent rapid exhumation of the Namche Barwa syntaxis. In the "tectonic aneurysm" model, the metamorphic massifs at the western and eastern Himalayan syntaxes are created by local feedback between tectonics and erosion; large-magnitude river incisions (by the Indus River which cuts across the western syntaxis and the Yarlung Tsangpo–Brahmaputra which cuts across the eastern syntaxis) focus deformation of weak crust, leading to lower crustal flow into the region. This creates a self-sustained failure of a normally strong boundary and rapid exhumation (Zeitler et al., 2014, and references therein). The Yarlung Tsangpo river capture has been proposed as the trigger for the tectonic aneurysm (Zeitler et al., 2001b; see also Robl et al., 2008). However, our data show that capture is at least 10 Ma older, and thus if such capture was routed through the Siang, it refutes the river capture as the trigger for the tectonic aneurysm, in agreement with the recent research of Wang et al (2014).

Acknowledgements

The authors thanks NERC (Natural Environment Research Council) for supporting this research through grants NE/F01807X/1 to Y.N. and NE/F017588/1 to R.R.P. Thanks are due to Marcelle BouDagher-Fadel and Paul Bown (University College London) for checking the Surma Basin samples for occurrence of foraminifera. L.B. warmly thanks Vanessa Pashley and Matt Horstwood (NERC Isotope Geosciences Laboratory) for support and advice with the LA U-Pb work. We thank two anonymous reviewers and the Editor An Yin for their constructive reviews and comments that helped to improve the manuscript significantly.

Appendix A. Supplementary Material

Supplementary material related to this article can be found online at http://dx.doi.org/101016/j.epsl.xxxx.xx.xxx.

References

Aikman, A.B., Harrison, T.M., Lin, D., 2008. Evidence for Early (> 44 Ma) Himalayan Crustal Thickening, Tethyan Himalaya, southeastern Tibet. Earth Planet. Sci. Lett. 274, 14–23.

Baksi, A.K., 1995. Petrogenesis and timing of volcanism in the Rajmahal flood basalt province, northeastern India. Chem. Geol., 121, 73–90.

Beaumont, C., Fullsack, P., Hamilton, J., 1992. Erosional control of active compressional orogens. In: McClay, K.R. (Ed.), Thrust Tectonics. Springer Netherlands, pp. 1–18.

Beaumont, C., Jamieson, R.A., Nguyen, M.H., Lee, B., 2001. Himalayan tectonics explained by extrusion of a low-viscosity crustal channel coupled to focused surface denudation. Nature 414, 738–742.

Bishop, P., 1995. Drainage rearrangement by river capture, beheading and diversion. Progr. Phys. Geogr. 19, 449–473.

Bracciali, L., Parrish, R.R., Horstwood, M.S.A., Condon, D.J., Najman, Y., 2013. U-Pb LA-(MC)-ICP-MS dating of rutile: New reference materials and applications to sedimentary provenance. Chem. Geol. 347, 82–101.

Brookfield, M.E., 1998. The evolution of the great river systems of southern Asia during the Cenozoic India–Asia collision: rivers draining southwards. Geomorphology 22, 285–312.

Burrard, S.G., Hayden, H.H., 1907. A Sketch of the Geography and Geology of the Himalaya Mountains and Tibet: The high peaks of Asia, 1. Superintendent government printing, India.

Cawood, P.A., Johnson, M.R.W., Nemchin, A.A., 2007. Early Palaeozoic orogenesis along the Indian margin of Gondwana: Tectonic response to Gondwana assembly. Earth Planet. Sci. Lett. 255, 70–84.

Chirouze, F., Huyghe, P., van der Beek, P., Chauvel, C., Chakraborty, T., Dupont-Nivet, G., Bernet, M., 2012a. Tectonics, exhumation, and drainage evolution of the eastern Himalaya since 13 Ma from detrital geochemistry and thermochronology, Kameng River Section, Arunachal Pradesh. Geol. Soc. Am. Bull. 125, 523–538.

Chirouze, F., Dupont-Nivet, G., Huyghe, P., Beek, P.v.d., Chakraborti, T., Bernet, M., Erens,V., 2012b. Magnetostratigraphy of the Neogene Siwalik Group in the far eastern Himalaya: Kameng section, Arunachal Pradesh, India. J. Asian Earth Sci. 44, 117–135.

Chiu, H.-Y.,Chung, S.-L., Wu, F.-Y., Liu, D., Liang, Y.-H., Lin, I.-J., Iizuka, Y., Xie, L.-W., Wang, Y., Chu, M.-F., 2009. Zircon U-Pb and Hf isotopic constraints from eastern Transhimalayan batholiths on the precollisional magmatic and tectonic evolution in southern Tibet. Tectonophysics 477, 3–19.

Chu, M.-F., Chung, S.-L., Song, B., Liu, D.-Y., O'Reilly, S.Y., Pearson, N.J., Ji, J.-Q., Wen, D.-J., 2006. Zircon U–Pb and Hf isotope constraints on the Mesozoic tectonics and crustal evolution of southern Tibet. Geology 34, 745–748.

Chu, M.-F., Chung, S.-L., O'Reilly, S.Y., Pearson, N.J., Wu, F.-Y., Li, X.-H., Liu, D., Ji, J., Chu, C.-H., Lee, H.-Y., 2011. India's hidden inputs to Tibetan orogeny revealed by Hf isotopes of Transhimalayan zircons and host rocks. Earth Planet. Sci. Letters, 307, 479–486.

Chung, S.-L., Chu, M.-F., Ji, J.-Q., O'Reilly, S.Y., Pearson, N.J., Liu, D.-Y., Lee, T.-Y., Lo, C.-H., 2009. The nature and timing of crustal thickening in Southern Tibet: Geochemical and zircon Hf isotopic constraints from postcollisional adakites. Tectonophysics 477, 36–48.

Cina, S.E., Yin, A., Grove, M., Dubey, C.S., Shukla, D.P., Lovera, O.M., Kelty, T.K., Gehrels, G.E., Foster, D.A., 2009. Gangdese arc detritus within the eastern Himalayan Neogene foreland basin: Implications for the Neogene evolution of the Yalu-Brahmaputra River system. Earth Planet. Sci. Lett. 285, 150–162.

Clark, M.K., Schoenbohm, L.M., Royden, L.H., Whipple, K.X., Burchfiel, B.C., Zhang, X., Tang, W., Wang, E., Chen, L., 2004. Surface uplift, tectonics, and erosion of eastern Tibet from large-scale drainage patterns. Tectonics 23, TC1006.

Comas-Cufí, M., Thió-Henestrosa, S., 2011. CoDaPack 2.0: a stand-alone, multiplatform compositional software, CoDaWork'11: 4th International Workshop on Compositional Data Analysis, Sant Feliu de Guíxols, Spain.

Copeland, P., Harrison, T.M., Pan, Y., Kidd, W., Roden, M., Zhang, Y., 1995. Thermal evolution of the Gangdese batholith, southern Tibet: a history of episodic unroofing. Tectonics 14, 223–236.

Deb, P.K., Howladar, M.F., Miah, M.I., Faruque, M.O., Islam, M.S., Mia, M.B., Quamruzzaman, C., 2014. Structural Interpretation of Fenchuganj Gas Field. J. Eng. Geol. Hydrog. 2, 29–36.

DeCelles, P., Gehrels, G., Quade, J., LaReau, B., Spurlin, M., 2000. Tectonic implications of U-Pb zircon ages of the Himalayan orogenic belt in Nepal. Science 288, 497–499.

DeCelles, P.G., Gehrels, G.E., Najman, Y., Martin, A.J., Carter, A., Garzanti, E., 2004. Detrital geochronology and geochemistry of Cretaceous–Early Miocene strata of Nepal: implications for timing and diachroneity of initial Himalayan orogenesis. Earth Planet. Sci. Lett. 227, 313–330.

Dickinson, W.R., 1982. Composition of sandstones in circum-Pacific subduction complexes and fore-arc basins. A.A.P.G. Bull. 66, 121–137.

England, P.C., Richardson, S.W., 1977. The influence of erosion upon the mineral fades of rocks from different metamorphic environments. J. Geol. Soc. 134, 201–213.

Evans, P., 1932. The Tertiary succession in Assam. Transactions in Mineralogy Geology and Metallurgy Institute of India 30, 174–233.

Galy, V., France-Lanord, C., Peucker-Ehrenbrink, B., Huyghe, P., 2010. Sr-Nd-Os evidence for a stable erosion regime in the Himalaya during the past 12 Myr. Earth Planet. Sci. Lett. 290, 474–480.

Garzanti, E., Vezzoli, G., 2003. A Classification of Metamorphic Grains in Sands Based on their Composition and Grade. J. Sed. Res. 73, 830–837.

Garzanti, E., Andò, S., France-Lanord, C., Vezzoli, G., Censi, P., Galy, V., Najman, Y., 2004. Mineralogical and chemical variability of fluvial sediments: 1. Bedload sand (Ganga-Brahmaputra, Bangladesh). Earth Planet. Sci. Lett. 299, 368–381.

Gehrels, G., DeCelles, P., Martin, A., Ojha, T., Pinhassi, G., Upreti, B., 2003. Initiation of the Himalayan orogen as an early Paleozoic thin-skinned thrust belt. GSA Today 13, 4–9.

Gehrels, G.E., Kapp, P., DeCelles, P., Pullen, A., Blakey, R., Weislogel, A., Ding, L., Guynn, J., Martin, A., McQuarrie, N., Yin, A., 2011. Detrital zircon geochronology of pre-Tertiary strata in the Tibetan-Himalayan orogen. Tectonics 30, TC5016.

Guo, L., Zhang, H.-F., Harris, N., Pan, F.-B., Xu, W.-C., 2011. Origin and evolution of multi-stage felsic melts in eastern Gangdese belt: Constraints from U-Pb zircon dating and Hf isotopic composition. Lithos 127, 54-67.

Guo, Z., Wilson, M., 2012. The Himalayan leucogranites: Constraints on the nature of their crustal source region and geodynamic setting. Gondw. Res. 22, 360–376.

Guo, Z., Wilson, M., Zhang, M., Cheng, Z., Zhang, L., 2013. Post-collisional, K-rich mafic magmatism in south Tibet: constraints on Indian slab-to-wedge transport processes and plateau uplift. Contrib. Mineral. Petrol. 165, 1311–1340.

Hallet, B., Molnar, P., 2001. Distorted drainage basins as markers of crustal strain east of the Himalaya. J. Geoph. Res.: Solid Earth 106, 13697–13709.

Harrison, T.M., Copeland, P., Kidd, W.S.F., Yin, A., 1992. Raising Tibet. Science 255, 1663–1670.

Henderson, A.L., Najman, Y., Parrish, R., BouDagher-Fadel, M., Barford, D., Garzanti, E., Andò, S., 2010. Geology of the Cenozoic Indus Basin sedimentary rocks: Paleoenvironmental interpretation of sedimentation from the western Himalaya during the early phases of India-Eurasia collision. Tectonics 29, TC6015.

Hodges, K.V., 2000. Tectonics of the Himalaya and southern Tibet from two perspectives. Geol. Soc. Am. Bull. 112, 324–350.

Hodges, K.V., Parrish, R.R., Searle, M.P., 1996. Tectonic evolution of the central Annapurna Range, Nepalese Himalayas. Tectonics 15, 1264–1291.

Hou, Z.-Q., Zheng, Y.-C., Zeng, L.-S., Gao, L.-E., Huang, K.-X., Li, W., Li, Q.-Y., Fu, Q., Liang, W., Sun, Q.-Z., 2012. Eocene-Oligocene granitoids in southern Tibet: Constraints on crustal anatexis and tectonic evolution of the Himalayan orogen. Earth Planet. Sci. Lett. 349–350, 38–52.

Hu, X., Jansa, L., Chen, L., Griffin, W.L., O'Reilly, S.Y., Wang, J., 2010. Provenance of Lower Cretaceous Wölong Volcaniclastics in the Tibetan Tethyan Himalaya: Implications for the final breakup of Eastern Gondwana. Sediment. Geol. 223, 193–205.

Ingersoll, R.V., Fullard, T.F., Ford, R.L., Grimm, J.P., Pickle, J.D., Sares, S.W., 1984. The effect of grain size on detrital modes; a test of the Gazzi-Dickinson point-counting method. J. Sed. Res. 54, 103–116.

Ji, W.-Q., Wu, F.-Y., Chung, S.-L., Li, J.-X. and Liu, C.-Z., 2009. Zircon U–Pb geochronology and Hf isotopic constraints on petrogenesis of the Gangdese batholith, southern Tibet. Chem. Geol. 262, 229–245.

Ji, W.-Q., Wu, F.-Y., Liu, C.-Z., Chung, S.-L., 2012. Early Eocene crustal thickening in southern Tibet: New age and geochemical constraints from the Gangdese batholith. J. Asian Earth Sci. 53, 82–95.

Johnson, S.Y., Nur Alam, A.M., 1991. Sedimentation and tectonics of the Sylhet Trough, Bangladesh. Geol. Soc. Am. Bull. 103, 1513–1527.

Kohn, M.J., 2014. Himalayan Metamorphism and Its Tectonic Implications. Annu. Rev. Earth. Planet. Sci. 42, 381–419.

Lang, K.A., Huntington, K.W., 2014. Antecedence of the Yarlung-Siang-Brahmaputra River, eastern Himalaya. Earth Planet. Sci. Lett. 397, 145–158.

Liang, Y.-H., Chung, S.-L., Liu, D., Xu, Y., Wu, F.-Y., Yang, J.-H., Wang, Y., Lo, C.-H., 2008. Detrital zircon evidence from Burma for reorganization of the eastern Himalayan river system. Am. J. Sci. 308, 618–638.

Lietz, J.K., Kabir, J., 1982. Prospects And Constrainst Of Oil Exploration In Bangladesh, Fourth Offshore South East Asia Show. Society of Petroleum Engineers, Singapore, pp. 1–6.

Ma, L., Wang, Q., Wyman, D.A., Jiang, Z.-Q., Yang, J.-H., Li, Q.-L., Gou, G.-N., Guo, H.-F., 2013. Late Cretaceous crustal growth in the Gangdese area, southern Tibet: Petrological and Sr–Nd–Hf–O isotopic evidence from Zhengga diorite–gabbro. Chem. Geol. 349–350, 54-70.

Martin, A.J., Burgy, K.D., Kaufman, A.J., Gehrels, G.E., 2011. Stratigraphic and tectonic implications of field and isotopic constraints on depositional ages of Proterozoic Lesser Himalayan rocks in central Nepal. Precambrian Res. 185, 1–17.

McKenzie, N.R., Hughes, N.C., Myrow, P.M., Xiao, S., Sharma, M., 2011. Correlation of Precambrian,ÄìCambrian sedimentary successions across northern India and the utility of isotopic signatures of Himalayan lithotectonic zones. Earth Planet. Sci. Lett. 312, 471–483.

McQuarrie, N., Robinson, D., Long, S., Tobgay, T., Grujic, D., Gehrels, G., Ducea, M., 2008. Preliminary stratigraphic and structural architecture of Bhutan: Implications for the along strike architecture of the Himalayan system. Earth Planet. Sci. Lett. 272, 105–117.

Mo, X., Niu, Y., Dong, G., Zhao, Z., Hou, Z., Zhou, S., Ke, S., 2008. Contribution of syncollisional felsic magmatism to continental crust growth: a case study of the Paleogene Linzizong volcanic succession in southern Tibet. Chem. Geol. 250, 49–67.

Myrow, P.M., Hughes, N.C., Paulsen, T.S., Williams, I.S., Parcha, S.K., Thompson, K.R., Bowring, S.A., Peng, S.-C., Ahluwalia, A.D. 2003. Integrated tectonostratigraphic analysis of the Himalaya and implications for its tectonic reconstruction. Earth Planet. Sci. Lett. 212, 433–441.

Najman, Y., 2006. The detrital record of orogenesis: A review of approaches and techniques used in the Himalayan sedimentary basins. Earth-Sci. Rev. 74, 1–72.

Najman, Y., Bickle, M., BouDagher-Fadel, M., Carter, A., Garzanti, E., Paul, M., Wijbrans, J., Willett, E., Oliver, G., Parrish, R., Akhter, S. H., Allen, R., Andò, S., Chisty, E., Reisberg, L., Vezzoli, G., 2008. The Paleogene record of Himalayan erosion: Bengal Basin, Bangladesh. Earth Planet. Sci. Lett. 273, 1–14.

Najman, Y., Bickle, M., Garzanti, E., Pringle, M., Barfod, D., Brozovic, N., Burbank, D., Andò, S., 2009. Reconstructing the exhumation history of the Lesser Himalaya, NW India, from a multitechnique provenance study of the foreland basin Siwalik Group. Tectonics 28, TC5018.

Najman, Y., Appel, E., Boudagher-Fadel, M., Bown, P., Carter, A., Garzanti, E., Godin, L., Han, J., Liebke, U., Oliver, G., Parrish, R., Vezzoli, G., 2010. Timing of India-Asia collision: Geological, biostratigraphic, and palaeomagnetic constraints. J. Geophys. Res. 115, B12416.

Najman, Y., Allen, R., Willett, E. A. F., Carter, A., Barfod, D., Garzanti, E., Wijbrans, J., Bickle, M. J., Vezzoli, G., Andò, S., Oliver, G., Uddin, M. J., 2012. The record of Himalayan erosion preserved in the sedimentary rocks of the Hatia Trough of the Bengal Basin and the Chittagong Hill Tracts, Bangladesh. Basin Res. 24, 499–519.

Ojha, T., Butler, R., DeCelles, P., Quade, J., 2009. Magnetic polarity stratigraphy of the Neogene foreland basin deposits of Nepal. Basin Res. 21, 61–90.

Parrish, R.R., Hodges, V., 1996. Isotopic constraints on the age and provenance of the Lesser and Greater Himalayan sequences, Nepalese Himalaya. Geol. Soc. Am. Bull. 108, 904–911.

Reimann, K.-U., 1993. Geology of Bangladesh, Bontraeger, Berlin, 154 pp.

Robinson, D.M., DeCelles, P.G., Patchett, P.J., Garzione, C.N., 2001. The kinematic evolution of the Nepalese Himalaya interpreted from Nd isotopes. Earth Planet. Sci. Lett. 192, 507–521.

Robinson, R.A.J., Brezina, C.A., Parrish, R.R., Horstwood, M.S.A., Oo, N.W., Bird, M.I., Thein, M., Walters, A.S., Oliver, G.J.H., Zaw, K., 2014. Large rivers and orogens: The evolution of the Yarlung Tsangpo-Irrawaddy system and the eastern Himalayan syntaxis. Gondwana Res. 26, 112–121.

Robl, J., Stüwe, K., Hergarten, S., 2008. Channel profiles around Himalayan river anticlines: Constraints on their formation from digital elevation model analysis. Tectonics 27, TC3010.

Roybarman, A., 1983. Geology and hydrocarbon prospects of West Bengal. Petrol. Asia J. 6, 51–56.

Rubatto, D., Chakraborty, S., Dasgupta, S., 2012. Timescales of crustal melting in the Higher Himalayan Crystallines (Sikkim, Eastern Himalaya) inferred from trace element-constrained monazite and zircon chronology. Contrib. Mineral. Petrol.1–24.

Rüber, L., Britz, R., Kullander, S.O., Zardoya, R., 2004. Evolutionary and biogeographic patterns of the Badidae (Teleostei: Perciformes) inferred from mitochondrial and nuclear DNA sequence data. Molecular Phylog. Evol. 32, 1010–1022.

Searle, M.P., Noble, S.R., Cottle, J.M., Waters, D.J., Mitchell, A.H.G., Hlaing, T., Horstwood, M.S.A., 2007. Tectonic evolution of the Mogok metamorphic belt, Burma (Myanmar) constrained by U-Th-Pb dating of metamorphic and magmatic rocks. Tectonics 26, TC3014.

Searle, M.P., Cottle, J.M., Streule, M.J., Waters, D.J., 2010. Crustal melt granites and migmatites along the Himalaya: melt source, segregation, transport and granite emplacement mechanisms. GSA Sp. Paper 472, 219–233.

Seeber, L., Gornitz, V., 1983. River profiles along the Himalayan arc as indicators of active tectonics. Tectonophysics 92, 335–367.

Seward, D., Burg, J.-P., 2008. Growth of the Namche Barwa Syntaxis and associated evolution of the Tsangpo Gorge: Constraints from structural and thermochronological data. Tectonophysics 451, 282–289.

Singh, S.K., France-Lanord, C., 2002. Tracing the distribution of erosion in the Brahmaputra watershed from isotopic compositions of stream sediments. Earth Planet. Sci. Lett. 202, 645–662.

Singh, S.K., Rai, S.K., Krishnaswami, S., 2008. Sr and Nd isotopes in river sediments from the Ganga Basin: Sediment provenance and spatial variability in physical erosion. J. Geoph. Res.: Earth Surface 113, F03006.

Stüwe, K., Robl, J., Hergarten, S., Evans, L., 2008. Modeling the influence of horizontal advection, deformation, and late uplift on the drainage development in the India-Asia collision zone. Tectonics 27, TC6011.

Thomas, R.J., Jacobs, J., Horstwood, M.S.A., Ueda, K., Bingen, B., Matola, R., 2010. The Mecubúri and Alto Benfica Groups, NE Mozambique: Aids to unravelling ca. 1 and 0.5 Ga events in the East African Orogen. Precambrian Res. 178, 72–90.

Uddin, A., Lundberg, N., 1998. Cenozoic history of the Himalayan-Bengal system: Sand composition in the Bengal basin, Bangladesh. Geol. Soc. Am. Bull. 110, 497–511.

Uddin, A., Lundberg, N., 1999. A paleo-Brahmaputra? Subsurface lithofacies analysis of Miocene deltaic sediments in the Himalayan–Bengal system, Bangladesh. Sediment. Geol. 123, 239–254.

Uddin, A., Hames, W.E., Zahid, K.M., 2010. Laser ^{40}Ar/^{39}Ar age constraints on Miocene sequences from the Bengal basin: Implications for middle Miocene denudation of the eastern Himalayas. J. Geoph. Res.: Solid Earth 115, B07416.

Wang, P., Scherler, D. Liu-Zeng, J., Mey, J, Avouac, J-P, Y Zhang, Y.,Shi, D., 2014. Tectonic control of Yarlung Tsangpo gorge revealed by a buried canyon in southern Tibet. Science 346, 978–981.

Webb, A.A.G., Yin, A., Dubey, C.S., 2013. U-Pb zircon geochronology of major lithologic units in the eastern Himalaya: Implications for the origin and assembly of Himalayan rocks. Geol. Soc. Am. Bull. 125, 499–522.

Willett, S., Beaumont, C., Fullsack, P., 1993. Mechanical model for the tectonics of doubly vergent compressional orogens. Geology 21, 371–374.

Worm, H.-U., Ahmed, A.M.M., Ahmed, N.U., Islam, H.O., Huq, M.M., Hambach, U., Lietz, J., 1998. Large sedimentation rate in the Bengal delta: Magnetostratigraphic dating of Cenozoic sediments from northeastern Bangladesh. Geology 26, 487–490.

Wu, W., Xu, S., Yang, J., Yin, H., Lu, H., Zhang, K., 2010. Isotopic characteristics of river sediments on the Tibetan Plateau. Chem. Geol. 269, 406-413.

Xu, Y.-G., Yang, Q.-J., Lan, J.-B., Luo, Z.-Y., Huang, X.-L., Shi, Y.-R., Xie, L.-W., 2012.Temporal–spatial distribution and tectonic implications of the batholiths in the Gaoligong–Tengliang–Yinjiang area, westernYunnan: constraints from zircon U-Pb ages and Hf isotopes. J. Asian Earth Sci. 53, 151–175.

Yin, A., 2006. Cenozoic tectonic evolution of the Himalayan orogen as constrained by along-strike variation of structural geometry, exhumation history, and foreland sedimentation. Earth-Sci. Rev. 76, 1–131.

Yin, A., Dubey, C.S., Kelty, T.K., Webb, A.A.G., Harrison, T.M., Chou, C.Y., Célérier, J., 2010a. Geologic correlation of the Himalayan orogen and Indian craton: Part 2. Structural geology, geochronology, and tectonic evolution of the Eastern Himalaya. Geol. Soc. Am. Bull. 122, 360–395.

Yin, A., Dubey, C.S., Webb, A.A.G., Kelty, T.K., Grove, M., Gehrels, G.E., Burgess, W.P., 2010b. Geologic correlation of the Himalayan orogen and Indian craton: Part 1. Structural geology, U-Pb zircon geochronology, and tectonic evolution of the Shillong Plateau and its neighboring regions in NE India. Geol. Soc. Am. Bull. 122, 336–359.

Zeitler, P.K., Koons, P.O., Bishop, M.P., Chamberlain, C.P., Craw, D., Edwards, M.A., Hamidullah, S., Jan, M.Q., Khan, M.A., Khattak, M.U.K., Kidd, W.S.F., Mackie, R.L., Meltzer, A.S., Park, S.K., Pecher, A., Poage, M.A., Sarker, G., Schneider, D.A., Seeber, L., Shroder, J.F., 2001a. Crustal reworking at Nanga Parbat, Pakistan: Metamorphic consequences of thermal-mechanical coupling facilitated by erosion. Tectonics 20, 712–728.

Zeitler, P.K., Meltzer, A.S., Koons, P.O., Craw, D., Hallet, B., Chamberlain, C.P., Kidd,W.S.F., Park, S.K., Seeber, L., Bishop, M., Shroder, J., 2001b. Erosion, Himalayan Geodynamics, and the Geomorphology of Metamorphism. GSA Today 11, 4–8.

Zeitler, P.K., Meltzer, A.S., Brown, L., Kidd, W.S.F., Lim, C., Enkelmann, E., 2014. Tectonics and topographic evolution of Namche Barwa and the easternmost Lhasa Block. In: Nie, J., Hoke, G.D., Horton, B. (Eds.), Towards an improved understanding of uplift mechanisms and the elevation history of the Tibetan Plateau: GSA Sp. Paper. 507, 23–58.

Zeng, L., Gao, L.-E., Xoe, K., Liu-Zeng, J., 2011.Mid-Eocene high Sr/Y granites in the Northern Himalayan Gneiss Domes: melting thickened lower continental crust. Earth Planet. Sci. Lett. 303, 251–266.

Zhang, H.F., Xu, W.C., Guo, J.Q., Zong, K.Q., Cai, H.M, Yuan, H.L., 2007. Zircon U–Pb and Hf isotopic composition of deformed granite in the southern margin of the Gangdese belt, Tibet: evidence for early Jurassic subduction of Neo-Tethyan oceanic slab. Acta Petrol. Sinica 23, 1347–1353.

Zhang, J.Y., Yin, A., Liu,W.C., Wu, F.Y., Lin, D., Grove, M., 2012. Coupled U–Pb dating and Hf isotopic analysis of detrital zircon of modern rivers and from the Yalu River (YarlungTsangpo) drainage system in southern Tibet: constraints on the transport processes and evolution of Himalayan rivers. Geol. Soc. Am. Bull. 124, 1449–1473.

Zhu, D.-C., Zhao, Z.-D., Niu, Y., Mo, X.-X., Chung, S.-L., Hou, Z.-Q., Wang, L.-Q., Wu, F.-Y., 2011. The Lhasa Terrane: Record of a microcontinent and its histories of drift and growth. Earth Planet. Sci. Lett. 301, 241–255.